Transp Porous Med (2012) 93:363–379
DOI 10.1007/s11242-012-9956-5

Numerical Algorithms for Network Modeling of Yield Stress and other Non-Newtonian Fluids in Porous Media

Matthew Balhoff · Daniel Sanchez-Rivera · Alan Kwok · Yashar Mehmani · Maša Prodanović

Received: 21 November 2011 / Accepted: 31 January 2012 / Published online: 23 February 2012

Abstract Many applications involve the flow of non-Newtonian fluids in porous, subsurface media including polymer flooding in enhanced oil recovery, proppant suspension in hydraulic fracturing, and the recovery of heavy oils. Network modeling of these flows has become the popular pore-scale approach for understanding first-principles flow behavior, but strong nonlinearities have prevented larger-scale modeling and more time-dependent simulations. We investigate numerical approaches to solving these nonlinear problems and show that the method of fixed-point iteration may diverge for shear-thinning fluids unless sufficient relaxation is used. It is also found that the optimal relaxation factor is exactly equal to the shear-thinning index for power-law fluids. When the optimal relaxation factor is employed it slightly outperforms Newton's method for power-law fluids. Newton-Raphson is a more efficient choice (than the commonly used fixed-point iteration) for solving the systems of equations associated with a yield stress. It is shown that iterative improvement of the guess values can improve convergence and speed of the solution. We also develop a new Newton algorithm (Variable Jacobian Method) for yield-stress flow which is orders of magnitude faster than either fixed-point iteration or the traditional Newton's method. Recent publications have suggested that minimum-path search algorithms for determining the threshold pressure gradient (e.g., invasion percolation with memory) greatly underestimate the true threshold gradient when compared to numerical solution of the flow equations. We compare the two approaches and reach the conclusion that this is incorrect; the threshold gradient obtained numerically is exactly the same as that found through a search of the minimum path of throat mobilization pressure drops. This fact can be proven mathematically; mass conservation is only preserved if the true threshold gradient is equal to that found by search algorithms.

Keywords Pore-scale modeling · Non-Newtonian flow · Yield stress · Invasion percolation with memory · Threshold path

M. Balhoff (✉) · D. Sanchez-Rivera · A. Kwok · Y. Mehmani · M. Prodanović
Department of Petroleum & Geosystems Engineering, The University of Texas at Austin,
1 University Station, C0300, Austin, 78712-0300 TX, USA
e-mail: balhoff@mail.utexas.edu

List of Variables

$\mathbf{F}$	Vector of errors in pore mass balance (m^3/s)
g	Conductivity of pore throat (m^3)
J	Jacobian
k	Permeability (m^2)
L	Length of a pore throat or network model (m)
m	Consistency index ($Pa\,s^n$)
M	Number of pores in reduced, Variable Jacobian
n	Shear-thinning index
N	Number of pores in network model
P	Pressure (Pa)
Q	Flow rate (cm^3/s)
R	Radius of pore throat (cm)
v	Darcy velocity (m/s)
α	Shift coefficient for shear rate in porous media
ε	Shift factor of approximate solution of yield-stress flow
ϕ	Porosity
$\dot{\gamma}$	Shear rate (1/s)
$\dot{\gamma}_R$	Shear rate at the wall of pore throat (1/s)
ΔP^*	Match pressure drop for approximate solution of yield-stress flow (Pa)
ΔP_m	Mobilization pressure drop for yield-stress flow (Pa)
δ	Numerical parameter in forward difference approximation of derivative
$\delta\mathbf{P}$	Change in solution vector, P, for Newton's method (Pa)
∇P_T	Threshold gradient for yield-stress flow in porous media (Pa/m)
η	Non-Newtonian viscosity (Pa s)
η_0	Low shear rate viscosity (Pa s)
λ	Weighting factor for fixed-point iteration
λ_{opt}	Weighting factor that minimizes number of iterations
μ	Viscosity (Pa s)
μ_{app}	Apparent Newtonian viscosity (Pa s)
μ_{max}	Maximum viscosity for yield-stress fluids (Pa s)
τ	Shear stress (Pa)
$\tau_{1/2}$	Rheological parameter in Ellis model (Pa)
τ_R	Shear stress at the wall of pore throat (Pa)
τ_0	Yield stress (Pa)

1 Introduction

Flow of non-Newtonian fluids in porous media is important in many subsurface applications. For example, in enhanced oil recovery polymers are used to increase sweep efficiency and may even reduce residual oil saturation (Wang et al. 2000). Crosslinked polymer gels are used during hydraulic fracturing operations to help carry proppant particles to the fracture; these fluids are often reported as exhibiting a yield stress (May et al. 1997; Balhoff and Miller 2005). Heavy oils are shown to be non-Newtonian as well which may lead to unexpected recovery in reservoirs. Non-Newtonian flow in porous media is also important in other industries such as polymer processing in packed beds (Chabbra 2000) and injection molding (Bruschke and Advani 1990).

Pore-scale network modeling (Fatt 1956a,b,c; Blunt et al. 2002) is a tool used to investigate fundamental flow behavior in porous media and to upscale macroscopic properties for inclusion into macroscopic reservoir simulators. Network models view the porous medium as a collection of pores connected by throats. It has been used to study many different flow phenomena and has advanced to allow for quantitative modeling and in many cases, the models are imaged directly from real media (Bakke and Øren 1997; Sheppard et al. 2005; Prodanovic et al. 2006). Although network models only approximate the morphology of the void space (and therefore the flow physics), simulations are often found to closely match experimental data (Bryant and Pallatt 1996; Bakke and Øren 1997; Valvatne and Blunt 2004; Balhoff and Wheeler 2009; Joekar-Niasar et al. 2010)

For modeling non-Newtonian flow, the fluid is usually described by a theoretical rheological model. For fluids that are shear thinning (or thickening), the power-law, Ellis, and Carreau models are popular. For fluids that exhibit a yield stress, the Bingham, Herschel–Bulkley, and Casson models are often chosen. All of these models are typically employed because of their relative simplicity and a closed-form expression for flow rate versus pressure drop in a capillary tube (pore throat) can often be found. Fluids that are viscoelastic have properties of both an elastic solid and viscous fluid, but investigation of these fluids is outside of the scope of this study.

Flow of shear-thinning fluids in qualitative network models was performed by Sorbie et al. (1989); Shah and Yortsos (1995), and Shah et al. (1998). In all cases the networks were 2D or simple 3D networks. Lopez et al. (2003) performed network modeling of Carreau fluids using networks mapped from consolidated and unconsolidated media and showed good agreement to experimental data. Although an analytical solution for a Carreau fluid in a pore throat (represented as a capillary tube) is not available, they derived an approximate expression. Balhoff and Thompson (2006) modeled the flow of power-law and Ellis fluids in packed beds of uniform and polydisperse spheres. They also obtained good agreement with experiments and developed a new macroscopic model for shear-thinning fluids. Sochi and Blunt (2008) presented results for the flow of shear-thinning fluid in unconsolidated and consolidated media and obtained good agreement with experimental data.

Yield-stress fluids are characterized by a minimum pressure gradient to yield flow and therefore are more challenging to model. Sahimi (1993) modeled general nonlinear behavior analogous to yield-stress flow in qualitative 2D and 3D networks. Shah et al. (1995) modeled the flow of a Bingham fluid in 2D networks with a distribution of throat radii and obtained the threshold gradient required to initiate flow. Balhoff and Thompson (2004) modeled the flow of Bingham fluids in packed beds of spheres using physically-representative network models of sphere packs. They obtained qualitative results of the flow paths at and near the threshold gradient, determined the threshold pressure gradient, and developed macroscopic curves of Darcy velocity and pressure gradient. They obtained a good match with some experimental data. Balhoff (2004) extended the work to model the flow of Herschel–Bulkley fluids. Chen et al. (2005) modeled yield-stress fluids in 2D networks and extended the work to include multiphase flow. Sochi and Blunt (2008) and Sochi (2010) modeled Herschel–Bulkley fluids in networks based on real sand packs and Berea sandstones which compared well to experimental data. Finally, Balan et al. (2011) recently modeled foam flow in porous media and used expressions for flow rate that required a mobilization pressure drop. Their network model was analogous to yield-stress flow in porous media.

Despite growing interest in pore-scale modeling of non-Newtonian fluids, strong nonlinearities prevent its wide use in larger models, in time-dependent schemes, and in multiscale simulations. The system of nonlinear equations that arise can be difficult to solve and computationally slow. The two most common methods employed in network modeling for solving

the nonlinear equations are (1) fixed-point iteration and (2) Newton's method. Fixed-point iteration tends to be the more widely used method for non-Newtonian applications despite the expectation that it is slower and perhaps less stable (Chapra and Canale 2010). The advantage of fixed-point iteration is the relative simplicity and ease of coding. The alternative is to use Newton's method, which is the usual choice for solving systems of nonlinear equations (but surprisingly uncommon for non-Newtonian network modeling). Newton's method is widely known to converge quickly (quadratic near the root) when it converges. However, it has no general convergence criteria, can in theory converge to an undesired root, and requires computation of potentially difficult partial derivatives. In this article, we test both approaches and compare stability and speed of convergence.

Yield-stress fluids require special numerical improvements because they require a threshold pressure gradient to induce flow in a porous medium. In an individual pore throat, flow is only finite if the pressure drop exceeds the local mobilization pressure drop (ΔP_{m}). Physically, the fluid is solid in these throats and has an infinite viscosity. This formulation causes numerical difficulties near the threshold gradient because flow rate (as well as the partial derivative of flow rate) is zero in some throats leading to singular matrices in both the fixed point and Newton approaches. The usual way the problem is circumvented is to impose a high, but finite viscosity in those throats in which $\Delta P < \Delta P_{\mathrm{m}}$. For example, Sochi (2010) used the fixed-point iteration method and imposed a maximum viscosity of 10^{50} Pa s in the no-flow region.

Balhoff and Thompson (2004) and then Balan et al. (2011) employed Newton's method to solve the nonlinear equations associated with the flow of fluids characterized by a yield stress. The approach leads to a singular Jacobian if no adjustments are made to the flow equations. They circumvented the problem by using an approximation of maximum, constant viscosity in throats below the mobilization pressure drop. Their algorithm implemented a moderate maximum viscosity, which was then used as an initial guess for a subsequent iteration with slightly higher maximum viscosity. These iterations continued until the approximate solution was sufficiently close to the true solution (i.e., the pressure field resulted in mass conservation in all pores below the predetermined tolerance for the true set of nonlinear equations). Their approach was numerically stable and convergent for all fluids and properties employed.

For flow of yield-stress fluids in porous media, the goal is often the determination of the exact threshold pressure gradient and the qualitative pathway in which the fluid flows at the threshold. Solution to the nonlinear equations are difficult at the threshold gradient because nearly all throats contain unyielded flow. For example in the Balhoff and Thompson (2004) approach, if the maximum viscosity in the approximate equations is too high, the solution is a poor approximation to the real set of equations; if the maximum viscosity is too low, the Jacobian is poorly conditioned. Nonetheless, both Balhoff and Thompson (2004) and Sochi (2010) claim to successfully obtain the exact threshold pressure gradient and path by numerical solution of the flow equations.

Alternative approaches for finding the threshold gradient involve minimum threshold path (MTP) algorithms (Sochi and Blunt 2008) that find the connected path of pore throats that minimizes the sum of mobilization pressure drops. Kharabaf and Yortsos (1997) introduced the invasion percolation with memory algorithm (IPM) to find the threshold gradient, which was also used by Chen et al. (2005). Sochi (2010) developed an algorithm, path of minimum pressure (PMP), which was much faster but did not allow backtracking (i.e., throats on the threshold path advanced only forward in the direction of the pressure gradient). They showed the two methods gave similar results, but PMP sometimes had a higher threshold gradient because of the absence of backtracking. Most importantly, they concluded both IPM and PMP

gave much different results than their numerical algorithm and significantly underestimated the true threshold gradient.

A goal of this study is to investigate and develop numerical approaches for solving flow of purely viscous, non-Newtonian fluids (particularly yield-stress fluids) in network models of porous media, and compare stability and speed of convergence. In addition, we show that threshold pressure gradient and flow path found numerically are exactly the same as found using search algorithms, such as IPM, which contradicts the findings of Sochi (2010).

2 Model Development

2.1 Network Generation

In this study, we utilize network models mapped from two different types of porous media: computer-generated sphere packs and sandstones digitized from real media. The sphere packs are obtained using a collective rearrangement algorithm (Jodrey and Tory 1985) and have the advantage of fast generation and the ability to easily vary grain-size distribution and porosity. Network models of sandstones are more difficult to extract and pore-level properties are fixed. We use a network model constructed from a real, naturally occurring sandstone (Gani and Bhattacharya 2003) that was imaged using X-ray computed microtomography (Thompson et al. 2008).

Regardless of the medium used, it is mapped to a 3D, physically representative network model using a modified Delaunay tessellation (Al-Raoush et al. 2003). The resulting network captures the inherent heterogeneity and consists of pores (containing the pore volume) and connecting throats (accounting for resistance to flow). The permeability of each network can be varied through scaling (where the grain diameters are increased to increase permeability). Simulations are conducted for a sphere pack with 1,000 grains, 38% porosity, and a uniform grain radius 0.0529 cm. The resulting network has 4,070 pores and a permeability of 1.06×10^{-5} cm^2. The sandstone has 2,487 grains, 17% porosity, and grain radius of 0.0344 cm. The network has 9,463 pores and a permeability of 1.84×10^{-7} cm^2. Both networks have dimensions of 1 cm $\times$ 1 cm $\times$ 1 cm.

2.2 Flow Modeling

Single phase flow in pore networks is modeled by imposing mass conservation at pores with the connecting throats providing the resistance to flow ($\sum_i q_{ij} = 0$). If the flowing fluid is Newtonian, a linear relationship between flow rate and the connecting throats describes flow. A linear system of equations arises which can be directly solved to obtain pore pressures and throat flow rates. For non-Newtonian fluids the relationship for throat flow rate is nonlinear and a nonlinear system of equations arises. Although there are dozens of constitutive models that can be used to describe the rheology of purely viscous non-Newtonian fluids, a few of the more common models that have been employed in network modeling (along with flow equations in a capillary tube) are depicted in Table 1 and studied in this study.

2.2.1 Fixed-Point Iteration

The fixed-point iteration method is implemented here using an approach similar to Lopez et al. (2003) and Sochi (2010). We (1) guess an initial solution for pressure (e.g., solution to

Table 1 Flow equations for various constitutive models for non-newtonian flow in a capillary tube

Model	Constitutive equation	Cylindrical throat flow equation	Apparent Newtonian viscosity in pore throat
Newtonian	$\tau = \mu\,\dot{\gamma}$	$Q_{ij} = \frac{\pi R^4}{8\mu L}\Delta P$ $\frac{\partial Q_{ij}}{\partial P_i} = \frac{\pi R^4}{8\mu L}$	$\mu_{ij,\mathrm{app}} = \mu$
Power-law	$\tau = m\,\dot{\gamma}^n$	$Q_{ij} = \frac{n\pi R^{3+1/n}}{(3n+1)(2\,\mathrm{mL})^{1/n}}\Delta P^{1/n}$ $\frac{\partial Q_{ij}}{\partial P_i} = \frac{\pi R^{3+1/n}}{(3n+1)(2\,\mathrm{mL})^{1/n}}\Delta P^{1/n-1}$	$\mu_{ij,\mathrm{app}} = m^{1/n}\left(\frac{3n+1}{4n}\right)\left(\frac{R\Delta P}{2\mathrm{L}}\right)^{1-1/n}$
Ellis	$\tau = \frac{\eta_0}{1+\left\lvert\frac{\tau}{\tau_{1/2}}\right\rvert^{\alpha-1}}\dot{\gamma}$	$Q_{ij} = \frac{\pi R^3\tau_R}{4\eta_0}\left[1+\frac{4}{\alpha+3}\left(\frac{\tau_R}{\tau_{1/2}}\right)\right]^{\alpha-1}$ $\frac{\partial Q_{ij}}{\partial P_i} = \frac{\pi R^4}{8\eta_0 L} + \frac{\alpha\pi R^3}{\eta_0(\alpha+3)\tau_{1/2}}\left(\frac{R}{2\mathrm{L}}\right)^{\alpha}\Delta P^{\alpha-1}$	$\mu_{ij,\mathrm{app}} = \eta_0\left[1+\frac{4}{\alpha+3}\left(\frac{\tau_R}{\tau_{1/2}}\right)\right]^{1-\alpha}$
Bingham	$\tau = \tau_0 + m\,\dot{\gamma}$	$Q_{ij} = \frac{\pi R^4}{8\,\mathrm{mL}}\Delta P$ $\left[1-\frac{4}{3}\left(\frac{2\mathrm{L}\tau_0}{\Delta\mathrm{PR}}\right)+\frac{1}{3}\left(\frac{2L\tau_0}{\Delta\mathrm{PR}}\right)^4\right]$ $\frac{\partial Q_{ij}}{\partial P_i} = \frac{\pi R^4}{8\,\mathrm{mL}} - 2\pi L^3\tau_0^4\Delta P^{-4}$	$\mu_{ij,\mathrm{app}} =$ $\left[1-\frac{4}{3}\left(\frac{2L\tau_0}{\Delta\mathrm{PR}}\right)+\frac{1}{3}\left(\frac{2\mathrm{L}\tau_0}{\Delta\mathrm{PR}}\right)^4\right]^{-1}$
Herschel–Bulkley	$\tau = \tau_0 + m\,\dot{\gamma}^n$	$Q_{ij} = \frac{\pi R^3(\tau_R-\tau_0)^{1/n+1}}{m^{1/n}\tau_R^3}$ $\left[\frac{(\tau_R-\tau_0)^2}{1/n+3}+\frac{2\tau_0(\tau_R-\tau_0)}{1/n+2}+\frac{\tau_0^2}{1/n+1}\right]\left[\frac{(\tau_R-\tau_0)^2}{1/n+3}+\frac{2\tau_0(\tau_R-\tau_0)}{1/n+2}+\frac{\tau_0^2}{1/n+1}\right]^{-1}$ $\frac{\partial Q_{ij}}{\partial P_i} \approx \frac{Q_{ij}(P_i+\delta)-Q_{ij}(P_i)}{\delta}$	$\mu_{\mathrm{app},ij} = \frac{m^{1/n}\tau_R^4}{4(\tau_R-\tau_0)^{1/n+1}}$
General fluid	$\tau = \eta\left(\dot{\gamma}\right)\dot{\gamma}$	$Q_{ij} = \frac{\pi R^3\dot{\gamma}}{3} - \frac{\pi}{3}\int_0^{\gamma_R}\eta^3\dot{\gamma}^3 d\dot{\gamma}$ $\frac{\partial Q_{ij}}{\partial P_i} \approx \frac{Q_{ij}(P_i+\delta)-Q_{ij}(P_i)}{\delta}$	$\mu_{ij,\mathrm{app}} = \frac{\pi R^4}{8Q_{ij}L}$

$\Delta P = P_i - P_j,\ \tau_R = \frac{\Delta P R}{2L}$

Newtonian equations); (2) calculate apparent, Newtonian viscosity in each throat based on the current guess of throat pressure drop (see Table 1); (3) solve the linear system of equations (biconjugate gradient solver used in this study) to update pore pressures; (4) repeat steps 2 and 3 using the new pressures and iterate on the solution until convergence is achieved. If the fluid exhibits a yield stress, a maximum viscosity of 10^{50} Pa s is allowed as used by Sochi (2010). Table 1 includes the apparent viscosity equations in capillary tubes (throats) for a current guess of pressure drop for various rheological models.

2.2.2 *Newton's Method*

Newton's method is implemented as was done by Balhoff and Thompson (2004) and Balan et al. (2011). We (1) guess an initial solution for pore pressure (e.g., solution to Newtonian equations); (2) Calculate the Jacobian (J) of partial derivatives and the error in mass balance in pores ($\mathbf{F}$); (3) solve the system of equations $J\boldsymbol{\delta}\mathbf{P} = -\mathbf{F}$; (4) Update the guess of pore pressures $P = P + \boldsymbol{\delta}\mathbf{P}$; and (5) iterate until the relative error in the norm of $\mathbf{F}$, $\|\mathbf{F}\|_2$, is below the specified tolerance. Table 1 shows the partial derivatives for flow in a capillary tube for various rheological models; they can be taken numerically when an analytical solution is not amenable.

For yield-stress fluids, an approximate flow equation is implemented so that small, but finite flow occurs in unyielded throats. The flow equation is linear with a small slope below $\Delta P^* = \Delta P_{\mathrm{m}}(1+\varepsilon)$. Above ΔP^* the flow equation is exactly the same as the actual equations

(Balhoff and Thompson 2004). This allows for evaluation of a non-singular Jacobian and a system of linear equations that can be solved robustly. The approximate equations for Bingham flow are written as:

$$Q = \frac{\pi R^4}{8\mu L}\Delta P\left[1 - \frac{4}{3}\left(\frac{2\tau_0 L}{\Delta P R}\right) + \frac{1}{3}\left(\frac{2\tau_0 L}{\Delta P R}\right)^4\right] \quad \text{if} \quad \Delta P > \Delta P^*$$
$$Q = \frac{\pi R^4}{8\mu_{\max} L}\Delta P \quad \text{if} \quad \Delta P \leq \Delta P^* \tag{1}$$

We refer to four types of pores that may be observed in the network for yield-stress flow. These pores may be found at an intermediate iteration or (in some instances) at the final, converged solution:

1. *Inactive pores* These pores are not part of any connected path in the network. All of the throats connected to the pore have a pressure drop below the mobilization pressure drop (ΔP_{m}).
2. *Isolated clusters* These pores are connected to other pores by throats with pressure drops above the mobilization pressure drops. However, the isolated cluster is not part of a connected path across the network. These pores are formed as a result of an incorrect guess in a Newton iteration or because flow through the cluster is so small that it falls below the specified tolerance.
3. *Dead end pores* The pores or clusters of pores are attached to a connected path, but lead to a dead end. Mass is not conserved in these clusters of pores since flow is finite on one end but zero on the other.
4. *Connected path* These pores are part of a connected path of pores spanning the inlet and outlet of the network. Mass is conserved in the connected path(s).

Once the system of equations are solved using the approximate model equations, the solution is used as an improved initial guess for pore pressures. The problem is re-solved by reducing ε and using the new ΔP^* (Balhoff and Thompson 2004) to find a more accurate pressure field. This is continued until ΔP^* is close to the mobilization pressure drop (ΔP_{m}) and mass conservation is preserved (below the specified tolerance) for the "true" system of equations. This pressure field is then taken as the solution. All of the throats with pressure drops above the mobilization pressure drop are "open" to flow; these throats should form connected paths across the network (otherwise mass balance would not be preserved locally). At the threshold pressure gradient, a single path of throats is open that connects the inlet and outlet of the network.

Upon convergence, some throats may appear open that are not part of the connected path (isolated clusters). This is physically impossible as it would violate mass balance (flow into any pore from a throat must exit through others). Close inspection shows that in these situations, flow rates are so small that they are below the specified tolerance for mass conservation and ΔP is only infinitesimally greater than the mobilization pressure drop. These isolated throats do not affect the numerical value of Darcy velocity or global mass balance in the network, but may give misleading values of the number of throats open and/or the flow paths. A search for any isolated throats is performed and they are discarded. It should be noted that these isolated pores/throats cannot be discarded in the iterative routine if local mass balance on the pore is above the specified tolerance, even if global mass balance (total flow into the network model equals flow out of the model) is found.

2.2.3 Variable Jacobian Newton's Method

The traditional Newton's method converges easily if the imposed pressure gradient is significantly higher than the threshold pressure gradient. It is near the threshold gradient that the system of nonlinear equations becomes difficult to solve. The method then requires many Newton iterations, each involving the solution of a large system of poorly conditioned linear equations. Near the threshold gradient, most of the throats are closed to flow (i.e., $\Delta P < \Delta P_{\mathrm{m}}$) and significant computation time is wasted on updating pressure in pores connecting these throats.

Here, we develop the Variable Jacobian Method which adaptively reduces the size of the Jacobian in each Newton iteration. Based on the current guess of pore pressures, the $N \times N$ Jacobian of partial derivatives (J) and the error in pore mass balance ($\mathbf{F}$) is formed using the true Bingham or Herschel–Bulkley equations (Eq. 1 is not necessary for the variable Jacobian method). Many pores in the network may be only connected to throats that are closed to flow (inactive pores); therefore the entire row and column of the Jacobian corresponding to that pore is zero. We reduce the size of the Jacobian by removing all rows and columns corresponding to these "inactive" pores. The corresponding rows of $\mathbf{F}$ are also removed. The resulting $M \times M$ (where $M < N$) Jacobian can be 1–2 orders of magnitude smaller than the full Jacobian (and better conditioned) which makes solution of $J\boldsymbol{\delta}\mathbf{P} = -\mathbf{F}$ much faster and easier. The pore pressures are updated and the procedure repeated in the next Newton iteration with potentially a different-size, reduced Jacobian. The procedure is repeated until $\|\mathbf{F}\|_2 < \mathrm{tol}$. It should be noted that by reducing the tolerance, the Jacobian size can sometimes be reduced even further, but this may require more iterations on the linear solver.

For an intermediate guess of pore pressures, two types of active pores appear in the network: (1) those on a connected path from the inlet to the outlet (2) those that form an isolated cluster (formation of the Jacobian as described above and shrinking it, we have automatically discarded inactive pores). Thereby we are left with only isolated clusters and connected paths. Iteration on those pore pressures will, by mass balance, dictate a constant pressure on the isolated clusters. In addition, a unique solution, compatible with the boundary conditions, is found on the percolating clusters. The constant pressure solution for the isolated clusters, however, will be non-unique as they are boundary value problems with pure Neumann boundary conditions.

This causes the Jacobian matrix to be singular and solution to the system of equations ($J\boldsymbol{\delta}\mathbf{P} = -\mathbf{F}$) will be composed of two parts: a unique solution for the connected path and a non-unique solution for the isolated clusters. The non-unique part (obtained using an iterative linear solver) results in perturbations in the pressure values in the isolated pores which cause these pores to either (1) become inactive or (2) re-arrange and possibly become part of a connected path. If the pores become inactive, and we converge, the solution is unique. If the isolated clusters re-arrange, we continue the iterative process until they also become inactive or become part of a connected path. In either case the final solution will be unique, no isolated clusters will be present, and both local and global mass balance will be preserved. It should be noted that the intermediate iterations depend on the iterative linear solver employed; however, the final connected path(s) will be the same. Convergence occurs for all pressure gradients at and above the threshold gradient.

2.3 Threshold Path Algorithms

The threshold pressure gradient can be found using the previously described numerical techniques for solving flow in the network. This entails iterating on the applied pressure

gradient to determine the smallest pressure gradient that yields flow and forms a single flow path in the network. This approach was used in Balhoff and Thompson (2004); Sochi and Blunt (2008), and Balan et al. (2011). An alternative approach for finding the threshold gradient involves search algorithms for finding a minimum path of mobilization pressure drops.

$$\nabla P_{\mathrm{T}} = \frac{1}{L} \sum_{\min} \Delta P_{\mathrm{m},ij} \tag{2}$$

A number of search algorithms can be employed including invasion percolation with memory (IPM) and path of minimum pressure (PMP). Both methods were used by Sochi and Blunt (2008) to find the threshold path. Other methods could be borrowed from graph theory such as the well-known Djikstra's algorithm (Ahuja et al. 1993) and the Floyd–Warshall (F–W) algorithm (Ahuja et al. 1993). The details of these methods are given in the references, but are summarized here for completeness. Essentially the algorithms search all potential connecting paths between source and destination and find the one that has the smallest sum of mobilization pressure drops (Eq. 3). F–W is an "all pairs" algorithm so it determines the minimum path for any two pores in the entire network. As a result, it is slow and not practical for the current application (but still accurate). Djikstra's algorithm finds the minimum path between a single source and single destination. Therefore, for our application, we must loop through all inlet pores and all exit pore combinations to find the minimum of all source/destination combinations. IPM is a variant of Djikstra's algorithm but faster because it finds the minimum of all source/destinations. Finally, PMP is potentially the fastest algorithm because it only checks for throats that are in the direction of the pressure gradient, but because it does not allow backtracking it may lead to inaccuracies (Sochi 2010). F–W, Djikstra, and IPM all result in the same, true minimum path.

3 Results and Discussion

3.1 Fixed Point versus Newton

Stability and speed of convergence were investigated for the two approaches (fixed-point iteration and Newton's method) for solving the systems of nonlinear equations. Table 2 summarizes the computation time and number of iterations for fixed-point iteration versus Newton for power-law flow. Not surprisingly, Newton is the much faster method when no relaxation (λ) on fixed-point iteration is used and also requires far less iterations.

Table 2 also shows that fixed-point iteration (without relaxation) does not converge at all if the power-law index (n) is less than 0.5. For power-law indices below 1/2, convergence can be obtained through relaxation; pressures are updated by weighting the old and new guesses:

$$P^k = \lambda P^k + (1 - \lambda) P^{k-1} \tag{3}$$

where a value of $\lambda < 1$ improves convergence. It should be noted that several authors (Sorbie et al. 1989; Lopez et al. 2003; Sochi and Blunt 2008) present solution of shear-thinning fluids without mention of convergence problems or the need of a relaxation strategy. It is possible that one is implemented and not stated. Many of the presented results have shear-thinning indices above or near 0.5 and the more practical Carreau or Ellis models are often used

Table 2 Summary of computational efficiency (seconds) for power-law flow in the network model of the sphere pack and sandstone

Network	n	FP ($\lambda = 1$)	FP ($\lambda_{opt} = n$)	Newton
Sphere	0.9	3.2 (8)	1.6 (4)	2.7 (3)
	0.75	6.7 (17)	2.0 (4)	3.6 (4)
	0.501	2000 (4976)	2.8 (7)	5.3 (6)
	0.499	DNC[a]	2.9 (7)	5.3 (6)
	0.25	DNC	6.2 (10)	9.9 (9)
	0.1	DNC	DNC	46 (22)
Sandstone	0.9	18 (5)	9.8 (3)	9.6 (2)
	0.75	464 (132)	16 (4)	14 (3)
	0.501	>5000	25 (7)	24 (5)
	0.499	DNC	21 (6)	24 (5)
	0.25	DNC	DNC	81 (17)
	0.1	DNC	DNC	103 (21)

The number of iterations is included in *parenthesis*
[a] DNC indicates "does not converge"

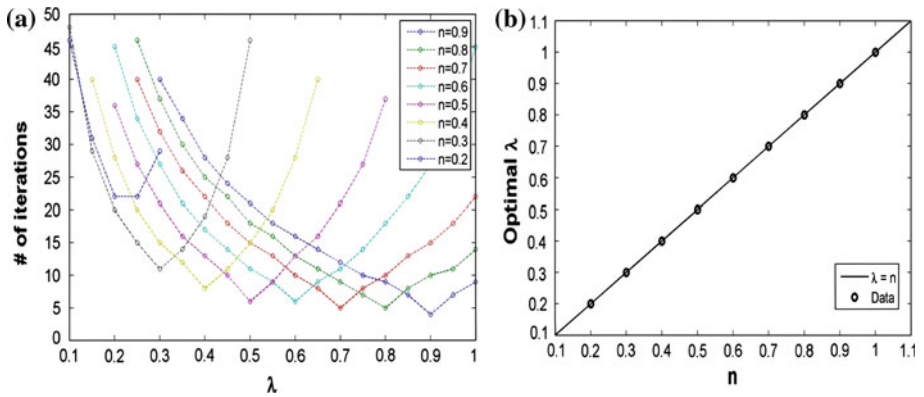

Fig. 1 **a** Iterations required for convergence versus λ for various power-law indices in the sphere pack. The minimum, λ_{opt}, was always found to be exactly equal to the power-law index and **b** λ_{opt} as a function of shear-thinning index for a power-law fluid in the network model created from a sphere pack

in place of a power-law fluid. These fluids have Newtonian plateaus which may add some stability to the problem that could allow convergence slightly below $n = 1/2$.

In general, relaxation strategies similar to that depicted in Eq. 3, require that the optimal $\lambda(\lambda_{opt})$ be found by trial and error. However, for power-law fluids we have found that λ_{opt} is exactly equal to the power-law index, n, as shown in Fig. 1a,b. Although the figure is shown for the sphere pack, the same relationship has been observed for several other networks. For yield-stress fluids, no universal equation for λ_{opt} has been found; it must be determined by trial and error.

As shown in Tables 2 and 3, Newton's method outperformed fixed-point iteration if no relaxation was used, but fixed-point slightly outperformed Newton if λ_{opt} was employed for power-law fluids. Although Newton's method is not guaranteed to converge in general, no problems were found provided the system of linear equations ($J\delta\mathbf{P} = -\mathbf{F}$) converges.

Table 3 Summary of computational efficiency (seconds) for Bingham flow in the network model of the spherepack and sandstone

Network	$\nabla P/\nabla P_T$	FP ($\lambda = 1$)	Newton	Variable Jacobian
Sphere	5.0	51 (23)	22 (9)	8.9 (8)
	2.0	DNC[a]	62 (26)	34 (16)
	1.50	DNC	69 (29)	41 (25)
	1.25	DNC	50 (21)	37 (35)
	1.1	DNC	40 (17)	19 (23)
	1.01	DNC	69 (29)	18 (21)
Sandstone	5.0	DNC	100 (21)	49 (22)
	2.0	DNC	133 (26)	53 (29)
	1.50	DNC	101 (20)	52 (28)
	1.25	DNC	170 (35)	54 (32)
	1.1	DNC	184 (38)	74 (44)
	1.01	DNC	337 (69)	62 (45)

The number of iterations is included in *parenthesis*
[a] DNC indicates "does not converge"

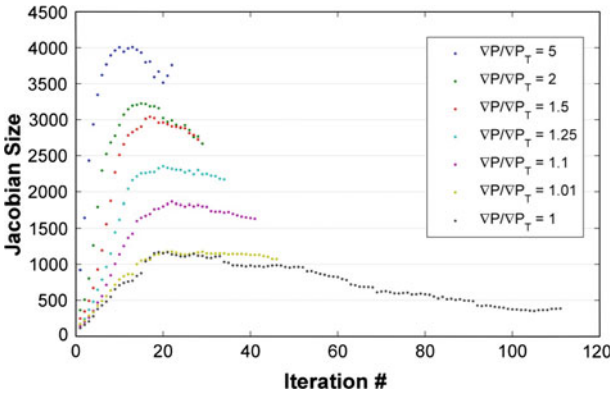

Fig. 2 Size of the Jacobian (M) with the number of iterations at various ratios of the pressure gradient to threshold gradient for the sandstone. The total number of pores (N) is 6,057

For yield-stress fluids, Newton's method is the preferred method over fixed-point iteration. Convergence of fixed-point iteration was difficult or impossible unless the pressure gradient was much higher than the threshold gradient. However, the new Variable Jacobian Method was also implemented and shown to be by far the superior approach over either fixed point or the traditional Newton method (Table 3) in terms of computation time. It converged in all cases tested and identical results for pore pressures were obtained as found using fixed-point iteration and Newton's method with a full Jacobian. The relatively small computation time is attributed to the small systems of linear equations that are solved (compared to the full Jacobian) during the Newton iterations, better condition number, and the lack of a need of an outer iteration on ε as was used in the traditional Newton's method with a full Jacobian. Fig. 2 shows that Jacobian size varies with each iteration and is also dependent on the pressure gradient.

Table 4 Summary of threshold gradient (Pa/cm) obtained via numerical solution and using search algorithms

Network	Variable Jacobian	F–W	Djikstra	IPM	PMP
SP_x[a]	55.95	55.95	55.95	55.95	55.95
	(13 s)	(6.1×10^3 s)	(130 s)	(0.39 s)	(0.39 s)
SP_y	56.65	56.65	56.65	56.65	56.65
	(24 s)	(6.1×10^3 s)	(130 s)	(0.38 s)	(0.39 s)
SP_z	49.75	49.75	49.75	49.75	49.75
	(20 s)	(6.1×10^3 s)	(140 s)	(0.38 s)	(0.39 s)
SS_x[b]	50.80	50.80	50.80	50.80	53.82
	(59 s)	(2.2×10^4 s)	(315 s)	(0.65 s)	(0.61 s)
S_y	65.28	65.28	65.28	65.28	69.17
	(95 s)	(2.2×10^4 s)	(113 s)	(0.63 s)	(0.53 s)
SS_z	69.93	69.93	69.93	69.93	73.08
	(119 s)	(2.2×10^4 s)	(218 s)	(0.63 s)	(0.54 s)

Computation times listed in seconds. Yield stress was 1 Pa
[a] SP is the network model generated from the sphere pack
[b] SS is the network model generated from the sandstone

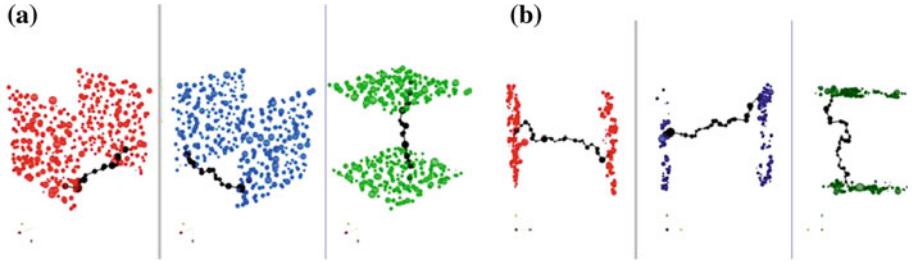

Fig. 3 Threshold path found via for **a** the sphere pack and **b** the sandstone in the *x*-, *y*-, and *z*-directions, respectively. The fluid had rheological properties $m = 1$ Pa s and $\tau_0 = 1$ Pa. Identical results were found using IPM, F–W, Djikstra, and the numerical approaches. The threshold path is in *black* and the boundary pores are in color

3.1.1 Threshold Gradient Determination for Yield-Stress Flow

Table 4 summarizes the threshold pressure gradients obtained for the networks using numerical algorithms (Newton's and fixed point) and the search algorithms (F–W, Djikstra, IPM, PMP). The solution using the numerical flow equations gives the exact same threshold gradient as F–W, Djikstra, and IPM. Likewise, the connecting flow path of throats across the network at the threshold gradient is exactly the same for all approaches. Figure 3 shows the flow path at the threshold pressure gradient in the sphere pack and sandstone.

Table 4 also shows that PMP method overestimates the threshold gradient for the sandstone. This is expected; as Sochi (2010) points out, PMP is only an approximate method because "backtracking" is not allowed. In the heterogeneous sandstone, the true flow path occasionally tracks in the direction opposite of the imposed pressure gradient. The more homogenous sphere pack does not require any backtracking and therefore PMP gives the same results as the more rigorous methods (IPM, Djikstra, and F–W). It should also be noted that the threshold path and pressure gradient are exactly the same regardless of the flow model

(Bingham, Herschel–Bulkley, Casson, etc.) implemented. This was discussed in Balan et al. (2011). Flow yields in a throat when the pressure drop exceeds ΔP_{m}; at the threshold gradient flow is infinitesimal and dynamic effects are not relevant (Chen et al. 2005). Therefore, the constitutive model used to describe flow above the throat mobilization pressure drop has no impact on the solution.

The agreement of the threshold flow path between IPM and numerical solution is in stark contrast to the conclusions presented by Sochi and Blunt (2008) and Sochi (2010). Sochi (2010) presents results that show both IPM and PMP significantly underestimate the numerical threshold gradient (by a factor of 2–3). An explanation for the disparity is provided in which it is claimed that (1) the threshold gradient of the entire network should be equal to the threshold gradient of the bottleneck (most resistant throat) of the path, (2) dynamic effects (viscosity) which is relevant above the threshold gradient affect the numerical solution at the threshold gradient, and (3) the tortuous path that fluid travels increases the threshold gradient.

However, those conclusions cannot be correct and violate basic material balance principles. Let us assume that the "true" threshold gradient ($\nabla P_{\mathrm{T,numerical}}$) were in fact greater than the threshold found from the minimum-path search algorithm ($\nabla P_{\mathrm{T,MTP}}$). This condition requires that the pressure drop across at least one throat along the true threshold flow path is greater than the throat mobilization pressure drop (ΔP_{m}), meaning flow must be finite in that throat(s). For mass balance to be preserved, flow would have to then be finite in connecting throats across the network (to insure flow in equals flow out of every pore in the network). But at the true threshold gradient, flow only first yields and is infinitesimal ($q = 0^{+}$). It is impossible then for the pressure gradient to be above the minimum-path pressure gradient and not yield flow.

In reality, the threshold gradient found via numerical solution (which conserves mass) must be equal to the gradient that minimizes the sum of mobilization pressure drops (as we found in Table 4). At the threshold pressure gradient, the pressure drop across each throat along the threshold flow path is exactly equal to the mobilization pressure drop in those throats. A mathematical proof is provided in the appendix which shows that the threshold gradient is equal to the sum of mobilization pressure drops on the threshold path.

It is unknown why Sochi (2010) obtains a numerical threshold gradient much higher than predicted by the search algorithms, but we propose one possible explanation. Above the threshold gradient, it is possible to obtain a pressure field during the iterative procedure that gives a single flow path across the network in addition to several isolated clusters of pores that do not form a path. If the applied pressure difference across the network is exactly equal to the sum of mobilization pressure drops on that path, the flow rate will be 0^{+} along that path and global mass balance is preserved. However, the result would only be an illusion of convergence because mass is not conserved locally in the isolated pore clusters. Mass balance must be preserved locally at all pores (at least below a specified, small tolerance) and if iterations were continued until this condition is met, one would find that a new path forms which yields at a lower pressure gradient—the same flow path and threshold gradient found from search algorithms.

4 Conclusions

A pore-scale network model has been used to investigate the numerical accuracy and efficiency of several algorithms used to study non-Newtonian flow in porous media with emphasis on shear-thinning fluids with and without a yield stress. The main conclusions of this study are summarized as follows:

- Fixed-point iteration does not always converge unless a sufficient relaxation coefficient (λ) is used that weights the old and new guesses of pore pressures. For power-law fluids, relaxation must be used for $n < 1/2$. Moreover, it is found that the optimum relaxation (λ_{opt}) for power-law fluids is exactly equal to the shear-thinning index, n. No universal relationship was found for yield-stress fluids.
- Fixed-point iteration slightly outperforms Newton's method for power-law fluids if λ_{opt} is employed. Fixed point usually did not converge for yield-stress fluids unless the pressure gradient was much higher than the threshold gradient. In these cases, a Newton strategy (traditional or variable) is faster and should be employed.
- A new Variable Jacobian Method is employed for the flow of yield-stress fluids. The method addresses the strong nonlinearities and slow computations observed for yield-stress flow by discarding inactive pores and reducing the size of the Jacobian in each Newton iteration. It is faster and more robust than either the fixed point or full Jacobian Newton algorithms for yield-stress problems.
- The threshold pressure gradient found using minimum-path search algorithms (e.g., IPM, Djikstra, and F–W) is exactly the same as found from numerical approaches for solving the nonlinear yield-stress flow equations. This is in stark contrast to the conclusions made by Sochi (2010). Local mass balance on each pore (as opposed to only global mass balance) must be preserved to insure convergence to the correct solution.

Acknowledgments This material is partially based upon work supported as part of the Center for Frontiers of Subsurface Energy Security, an Energy Frontier Research Center funded by the U.S. Department of Energy, Office of Science, Office of Basic Energy Sciences under Award Number DE-SC0001114. It was also funded by the Petroleum and Geosystems Engineering Department and the Yates Foundation.

Appendix

Definition (*simple path*) In graph theory a path is a sequence of vertices with one edge between two consecutive vertices. A path with no repeated vertices is called a simple path.

Definition (*minimum percolation potential*) Define the minimum percolation potential of a flowing system A to be the value of the following limit:

$$\lim_{q_{\text{A}} \to 0^+} \Delta P_{\text{A}} = \Delta P_{m_{\text{A}}}$$

Remark $\Delta P_{\text{A}}(q_{\text{A}}) : \mathbb{R}^+ \cup \{0\} \to \mathbb{R}^+ \cup \{0\}$ is a continuous, monotonically increasing function. Also for any system A we have: $\Delta P_{\text{A}} < \Delta P_{\text{m}_{\text{A}}} \Rightarrow q_{\text{A}} = 0$.

Lemma *Lemma given a finite serial sequence of elements* $(\text{e}_k)_{k=1}^N$, *if the elemental fluxes and potentials are denoted by* q_{e_k}, ΔP_{e_k} *and the minimum percolation potential of each element by* $\Delta P_{\text{m}_{\text{e}_k}}$ *then* $\forall \mathbb{R}^+ \ni \bar{\varepsilon}, \exists \mathbb{R}^+ \ni \overline{\sigma}$ *such that the following holds:*

$$0 < q_{\text{e}_k} < \overline{\sigma}, \forall k \Rightarrow 0 < \sum_{k=1}^{N} \Delta P_{\text{e}_k}(q_{\text{e}_k}) - \sum_{k=1}^{N} \Delta P_{\text{m}_{\text{e}_k}} < \bar{\varepsilon}$$

Proof For every element e_k we can write the following. Let $\text{R} \ni \bar{\varepsilon} > 0$ be arbitrary, then $\exists \text{R}^+ \sigma_k$ such that:

$$0 < q_{\text{e}_k} < \sigma_{\text{e}_k} \Rightarrow 0 < |\Delta P_{\text{e}_k} - \Delta P_{\text{m}_{\text{e}_k}}| = \Delta P_{\text{e}_k} - \Delta P_{\text{m}_{\text{e}_k}} < \frac{\bar{\varepsilon}}{N}$$

Taking $\overline{\sigma} = \min\{\sigma_{\mathrm{e}_k}\}_{k=1}^{N}$ we have:

$$0 < q_{\mathrm{e}_k} < \overline{\sigma}, \forall k \Rightarrow 0 < \Delta P_{\mathrm{e}_k} - \Delta P_{\mathrm{m}_{\mathrm{e}_k}} < \frac{\bar{\varepsilon}}{N}$$

Summing the right hand side of the above implication over k we get:

$$0 < q_{\mathrm{e}_k} < \overline{\sigma}, \forall k \Rightarrow 0 < \sum_{k=1}^{N} \Delta P_{\mathrm{e}_k}(q_{\mathrm{e}_k}) - \sum_{k=1}^{N} \Delta P_{\mathrm{m}_{\mathrm{e}_k}} < \bar{\varepsilon}$$

□

Corollary *Given system A as a finite serial sequence of elements* $(\mathrm{e}_k)_{k=1}^{N}$*, the percolation potential of the system is the following:*

$$\Delta P_{\mathrm{m_A}} = \sum_{k=1}^{N} \Delta P_{\mathrm{m}_{\mathrm{e}_k}}$$

Proof Since in such a system we have $q_{\mathrm{e}_1} = q_{\mathrm{e}_2} = \ldots = q_{\mathrm{e}_N} = q_{\mathrm{A}}$ and $\sum_{k=1}^{N} \Delta P_{\mathrm{e}_k}(q_{\mathrm{A}}) = \Delta P_{\mathrm{A}}(q_{\mathrm{A}})$, using lemma above let $\mathbb{R} \ni \bar{\varepsilon} > 0$ be arbitrary, then $\exists \mathbb{R}^{+} \ni \bar{\sigma}$ such that:

$$0 < q_{\mathrm{e}_k} < \overline{\sigma}, \forall k \Rightarrow 0 < \sum_{k=1}^{N} \Delta P_{\mathrm{e}_k}(q_{\mathrm{e}_k}) - \sum_{k=1}^{N} \Delta P_{\mathrm{m}_{\mathrm{e}_k}} < \bar{\varepsilon}$$

Which in combination with the foregoing yields:

$$0 < q_{\mathrm{A}} < \overline{\sigma} \Rightarrow 0 < \Delta P_{\mathrm{A}}(q_{\mathrm{A}}) - \sum_{k=1}^{N} \Delta P_{\mathrm{m}_{\mathrm{e}_k}} < \bar{\varepsilon}$$

This means that $\lim_{q_{\mathrm{A}} \to 0^{+}} \Delta P_{\mathrm{A}} = \sum_{k=1}^{N} \Delta P_{\mathrm{m}_{\mathrm{e}_k}}$. □

Theorem *Given a finite network system A, let the following be the set of all percolation* (*simple*) *paths through the system* (*we will drop the word "simple" herein*)*:*

$$D = \{l_i = (\mathrm{e}_k^i)_{k=1}^{N_i} : i = 1, 2, \ldots\}$$

Each path i is a sequence of elements $(\mathrm{e}_k^i)_{k=1}^{N_i}$*. Let* $F : D \to \mathbb{R}^{+}$ *be the following map:*

$$F(l_i) = \sum_{k=1}^{N_i} \Delta P_{\mathrm{m}_{\mathrm{e}_k^i}} = \Delta P_{\mathrm{m}_{l_i}}$$

The minimum percolation potential of A is:

$$\Delta P_{\mathrm{m_A}} = \inf \Re(F)$$

Proof The network is finite, therefore D and hence $\Re(F)$ is finite. Thus, $\Re(F)$ has a minimum $\Delta P_{\mathrm{m}_{l_g}}$ corresponding to at least one path l_g. For all values of q_{A}, l_{g} is open to flow, otherwise the corresponding ΔP_{A} is bigger than $\Delta P_{\mathrm{m}_{l_{\mathrm{g}}}}$ an thus it must be flowing which is a contradiction.

Now pick arbitrarily $\mathbb{R}^{+} \ni \bar{\varepsilon}$, then for l_{g}, from lemma, $\exists \mathbb{R}^{+} \ni \bar{\sigma}$ such that:

$$0 < q_{\mathrm{e}_k^{\mathrm{g}}} < \overline{\sigma}, \forall k \Rightarrow 0 < \sum_{k=1}^{N_{\mathrm{g}}} \Delta P_{\mathrm{e}_k^{\mathrm{g}}}(q_{\mathrm{e}_k^{\mathrm{g}}}) - \sum_{k=1}^{N_{\mathrm{g}}} \Delta P_{m_{\mathrm{e}_k^{\mathrm{g}}}} < \bar{\varepsilon}$$

Also for any network we have $q_{\mathrm{A}} \geq q_{\mathrm{e}_k^i} \forall k, i$, and every q_{A} corresponds to a flux sequence in l_{g} as $(q^*_{\mathrm{e}_k^{\mathrm{g}}})_{k=1}^{N_{\mathrm{g}}}$ for which we have $\Delta P_{\mathrm{A}} = \sum_{k=1}^{N_{\mathrm{g}}} \Delta P_{\mathrm{e}_k^{\mathrm{g}}}(q^*_{\mathrm{e}_k^{\mathrm{g}}})$. Now we can write:

$$
\begin{aligned}
&if \quad 0 < q_{\mathrm{A}} < \overline{\sigma} \Rightarrow 0 < q^*_{\mathrm{e}_k^{\mathrm{g}}} < \overline{\sigma}, \forall k \\
&\Rightarrow 0 < \sum_{k=1}^{N_{\mathrm{g}}} \Delta P_{\mathrm{e}_k^{\mathrm{g}}}(q^*_{\mathrm{e}_k^{\mathrm{g}}}) - \sum_{k=1}^{N_{\mathrm{g}}} \Delta P_{\mathrm{m}_{\mathrm{e}_k^{\mathrm{g}}}} < \bar{\varepsilon} \quad \Rightarrow \quad 0 < \Delta P_{\mathrm{A}} - \sum_{k=1}^{N_{\mathrm{g}}} \Delta P_{\mathrm{m}_{\mathrm{e}_k^{\mathrm{g}}}} < \bar{\varepsilon}
\end{aligned}
$$

Thus,

$$
\lim_{q_{\mathrm{A}} \to 0^+} \Delta P_{\mathrm{A}} = \sum_{k=1}^{N_{\mathrm{g}}} \Delta P_{\mathrm{m}_{\mathrm{e}_k^{\mathrm{g}}}} = \Delta P_{\mathrm{m}_{l_{\mathrm{g}}}} = \inf \Re(F)
$$

□

References

Ahuja, R.K., Magnanti, T.L., Orlin, J.B.: Network Flows: Theory, Algorithms, and Applications. 1st edn. Prentice Hall, Englewood Cliffs (1993)

Al-Raoush, R., Thompson, K.E., Willson, C.S.: Comparison of network generation techniques for unconsolodated porous media. Soil Sci. Soc. Am. J. **67**(6), 1687–1700 (2003)

Bakke, S., Øren, P.E.: 3-D pore-scale modelling of sandstones and flow simulations in the pore networks. SPE J. **2**(2), 136–149 (1997)

Balan, H., Balhoff, M., Nguyen, Q., Rossen, W.: Network Modeling of Gas Trapping and Mobility in Foam EOR. Energy and Fuels 25(9): 3974–3987 (2011)

Balhoff, M.T.: Modeling the flow of crosslinked guar gum in porous media. Polym. Prepr. **45**(2), 128–129 (2004)

Balhoff, M., Thompson, K.: A macroscopic model for shear-thinning flow in packed beds based on network modeling. Chem. Eng. Sci. **61**(2), 698–719 (2006)

Balhoff, M., Thompson, K.: Modeling the steady flow of yield-stress fluids in packed beds. AIChE J. **50**(12), 3034–3048 (2004)

Balhoff, M.T., Miller, M.J.: An analytical model for cleanup of yield-stress fluids in hydraulic fractures. SPE J. **10**(1), 3–11 (2005)

Balhoff, M.T., Wheeler, M.F.: A predictive pore scale model of non-darcy flow in porous media. SPE J. **v14**(4), 579–587 (2009)

Blunt, M., Jackson, M., Piri, M., Valvatne, P.: Detailed physics, predictive capabilities and macroscopic consequences for pore-network models of multiphase flow. Adv. Wat. Res. **25**(8-12), 1069–1089 (2002)

Bruschke, M.V., Advani, S.G.: A finite element/control volume approach to mold filling in anisotropic porous media. Polym. Compos. **11**, 398–405 (1990)

Bryant, S., Pallatt, N.: Predicting formation factor and resistivity index in simple sandstones. J. Petroleum Sci. Eng. **15**(2–4), 169–179 (1996)

Chabbra, R.P.: Bubbles, drops, and particles in non-newtonian fluids. CRC press, Boca Raton (2000)

Chapra, S., Canale, R.: Numerical methods for engineers, 6th edn. McGraw-Hill, Boston (2010)

Chen, M., Rossen, W., Yortsos, Y.: The flow and displacement in porous media of fluids with yield stress. Chem. Eng. Sci. **60**(15), 4183–4202 (2005)

Fatt, I.: The network model of porous media I. Capillary characreristics. Pet. Trans. AIME **207**, 144–159 (1956a)

Fatt, I.: The network model of porous media II. Dynamic properties of a single size tube network. Pet. Trans. AIME **207**, 160–163 (1956b)

Fatt, I.: The network model of porous media III. Dynamic properties of networks with tube radius distribution. Pet. Trans. AIME **207**, 164–181 (1956c)

Gani, M.R., Bhattacharya, J.P.: Bed-scale facies architecture of an ancient delta lobe deposit of the wall creek member, Central Wyoming, U.S.A., In: Proceedings of the AAPG Annual Convention & Exhibition, Salt Lake City, UT, 11–14 May (2003)

Jodrey, W., Tory, E.: Computer simulation of close random packing of equal spheres. Phys. Rev. A. **32**(4), 2347–2351 (1985)

Joekar-Niasar, V., Prodanović, M., Wildenschild, D., Hassanizadeh, S.M.: Network model investigation of interfacial area, capillary pressure and saturation relationships in granular porous media. Wat. Resour. Res. 46(6), W06526 (2010)

Kharabaf, H., Yortsos, Y.: Invasion percolation with memory. Phys. Rev. E. **55**(6), 7177–7191 (1997)

Lopez, X., Valvatne, P.H., Blunt, M.J.: Predictive network modeling of single-phase non-newtonian flow in porous media. J. ColloidInterf. Sci. **264**(1), 256–265 (2003)

May, E., Britt, K., Nolte, K: The effect of yield stress on fracture fluid cleanup. In: Paper SPE 38619 presented at the 1997 SPE Annual Technical Conference and Exhibition, San Antonio, Texas, 5–8 Oct 1997.

Prodanovic, M., Lindquist, W., Seright, R.: Porous structure and fluid partitioning in polyethylene cores from 3D X-ray microtomographic imaging. J. Colloid Interf. Sci. **298**(1), 282–297 (2006)

Sahimi, M.: Flow phenomena in rocks: from continuum models to fractals, percolation, cellular automata, and simulated annealing. Rev. Mod. Phys. **65**, 1393–1534 (1993)

Shah, C., Yortsos, Y.: Aspects of flow of power-law fluids in porous media. AIChE J. **41**, 1099–1112 (1995)

Shah, C., Kharabaf, H., Yortsos, Y.C.: Immiscible Displacements Involving Power-Law Fluids in Porous Media. In: Proceedings of the 7th UNITAR International Conference on Heavy Oils and Tar Sands, Beijing, China, 27–30 Oct (1998)

Shah, C., Kharabaf, H., Yortsos, Y.: In Flow and Displacement of Bingham Plastics in Porous Media. In: Proceedings of the 6th UNITAR Conference On Heavy Oils and Tar Sands, Houston, TX, 16 Feb (1995)

Sheppard, A., Sok, R., Averdunk, H.: improved pore-network generation methods. In: 19th International Symposium of the Society of Core Analysts. Society of Core Analysts, Austin, TX (2005)

Sochi, T., Blunt, M.: Pore-scale network modeling of Ellis and Herschel-Bulkley fluids. J. Petroleum Sci. Eng. **60**(2), 105–124 (2008)

Sochi, T.: Modelling the flow of yield-stress fluids in porous media. Trans. Porous Med. **85**, 489–503 (2010)

Sorbie, K., Clifford, P., Jones, E.: The rheology of pseudoplastic fluids in porous media using network modeling. J. Colloid Interf. Sci. **130**, 508–534 (1989)

Thompson, K., Willson, C., White, C., Nyman, S., Bhattacharya, J., Reed, A.: Application of a new grain-based reconstruction algorithm to microtomography images for quantitative characterization and flow modeling. SPE J. **13**(2), 164–176 (2008)

Valvatne, P.H., Blunt, M.J.: Pore-scale modeling of longitudinal dispersion. Wat. Resour. Res. **40**, W07406 (2004)

Wang, D., Cheng, J., Yang Q., Gong W., Li Q., Chen, F.: Viscous-elastic polymer can increase microscale displacement efficiency in cores. In: SPE 63227, presented at the 2000 SPE Annual Technical Conference and Exhibition held in Dallas, Texas, 1–4 Oct (2000)